Redox Sites in Zeolites

DOI: 10.1002/ange.200902199

Unambiguous Observation of Electron Transfer from a Zeolite Framework to Organic Molecules**

*Lu Li, Xue-Song Zhou, Guo-Dong Li, Xiao-Liang Pan, and Jie-Sheng Chen**

Zeolites are crystalline aluminosilicates with microporous structures. These materials have been widely used in the field of heterogeneous catalysis.[1] In most catalytic reactions involving a zeolite catalyst, the acidic sites of the zeolite play a pivotal role; hence, much attention has been paid to the nature of the acidic sites and the interactions of these sites with organic molecules.[2] The oxidation states of the framework atoms (Si, Al, and O) are thought to remain unchanged during acid-catalyzed reaction processes. However, electron loss from the zeolite framework may occur when a zeolite is subjected to a high temperature[3] or high-energy γ-ray (or X-ray) irradiation.[4] Electron transfer between zeolites and occluded molecules has also been proposed previously.[5] The electron-donating ability of the zeolite framework[6] and the ability of zeolites to generate organic radical cations[7] have been established by several research groups. Although it is recognized that electrons may be transferred between zeolites and occluded guest species, the nature of the electron donor/acceptor in zeolites has not yet been elucidated clearly, and the whereabouts of the electrons/holes formed in the electron-transfer process has been under intense debate.[5,7] In particular, when zeolites act as electron donors, only occluded molecules that accept electrons from zeolites can be observed to change, whereas a difference in the zeolite framework can hardly be detected after the electron-transfer process.

Herein, we demonstrate that aluminosilicate zeolites in the protonated form lose their framework electrons when alkyl bromides are introduced into the pores of the zeolites. The loss of the framework electrons results in paramagnetic centers, which function as single-electron redox sites and can be detected by electron paramagnetic resonance (EPR) spectroscopy. More importantly, this process of electron transfer accompanies the acid-catalyzed reaction between zeolites and alkyl bromides; thus, framework electron transfer of acidic zeolites should be considered to be partially responsible for the formation of some of the organic products during acid-catalyzed reactions involving zeolites.

A mixture of the dehydrated zeolite HY (protonated zeolite Y with a framework Si/Al ratio of 2.46; see Figure S2 in the Supporting Information) and ethyl bromide was stirred and heated at reflux in an airtight vessel at 50 °C under argon for 24 h. We refer to this process as the "liquid–solid" (L–S) reaction. After the L–S reaction, the HY material (designated Y–R) was orange in liquid ethyl bromide and turned light pink upon the removal of the liquid alkyl bromide with a liquid-nitrogen trap (see Figure S3 in the Supporting Information). The liquid ethyl bromide remained colorless throughout the whole reaction process, both before and after trapping; in the gas phase of the product of the catalytic reaction, a small quantity of ethane was detected, besides ethene and hydrogen bromide. Figure 1a shows the EPR spectrum of the HY zeolite under Ar after the L–S reaction and the removal of liquid ethyl bromide (see also Figure S4 in the Supporting Information). The appearance of a distinct singlet signal ($g = 2.0035$, $\Delta H = 11.0$ G) indicates that paramagnetic centers are generated in the zeolite during the L–S reaction. The concentration of the paramagnetic centers increases with the L–S reaction temperature (Figure 1b).

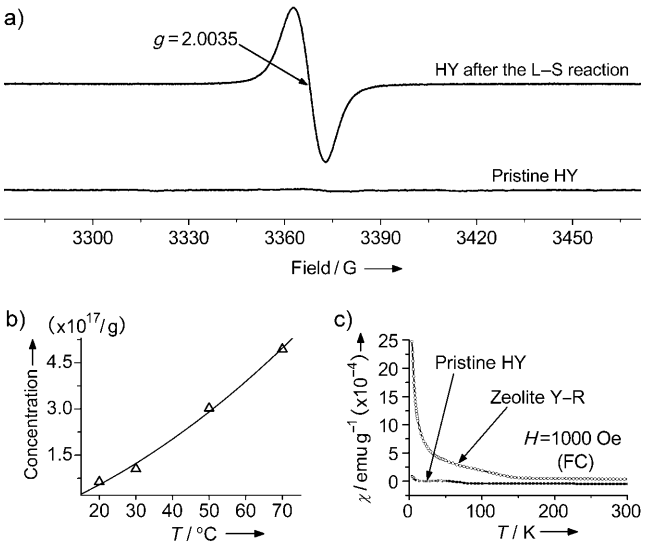

Figure 1. a) Room-temperature X-band EPR spectra of pristine HY and an HY sample after the L–S reaction at 50 °C under argon. b) Plot of the concentration of paramagnetic centers generated versus the L–S reaction temperature. c) Temperature dependence of the mass magnetic susceptibilities of pristine HY and an HY sample after the L–S reaction (Y–R).

[*] L. Li, X. S. Zhou, Prof. G. D. Li, X. L. Pan
State Key Laboratory of Inorganic Synthesis and Preparative Chemistry, College of Chemistry
Jilin University, Changchun 130012 (China)
L. Li, X. S. Zhou, Prof. J. S. Chen
School of Chemistry and Chemical Engineering
Shanghai Jiao Tong University, Shanghai 200240 (China)
Fax: (+86) 21-5474-1297
E-mail: chemcj@sjtu.edu.cn

[**] This research was supported financially by the National Natural Science Foundation of China (20731003) and the National Basic Research Program of China (2007CB613303)

Supporting information for this article is available on the WWW under http://dx.doi.org/10.1002/anie.200902199.

For comparison, we also recorded the EPR spectra of NaY after the L–S reaction, pristine HY, and ethyl bromide, but these materials were found to be EPR silent. The magnetic susceptibilities in emu per gram of the zeolite Y–R and pristine HY were recorded at 1000 Oe over the temperature range 4–300 K (Figure 1c). At room temperature, pristine HY shows a diamagnetic susceptibility value (-4.8×10^{-5} emu g^{-1}), whereas the zeolite Y–R shows a paramagnetic susceptibility value (3.8×10^{-5} emu g^{-1}), in agreement with the EPR results. Clearly, the singlet EPR signal of the HY zeolite after the L–S reaction is not due to the presence of paramagnetic impurities (such as Fe) in either the catalyst (HY) or the reactant (ethyl bromide). We also used Hβ (protonated zeolite beta) and H-mordenite (protonated zeolite mordenite) as catalysts in place of the zeolite HY and recorded the EPR spectra of these two zeolites after treatment with various alkyl halides, such as propyl bromide, butyl bromide, hexyl bromide and butyl chloride. The same singlet signal was observed in the spectra of all catalyst samples (see Figures S5–S7 in the Supporting Information). This observation demonstrates that the EPR signal can not be attributed to the presence of organic radicals, because otherwise different signals should appear, as the features of organic radicals formed in zeolites (and consequently the corresponding EPR signals) are strongly dependent on the guest reactant molecule and the structure of the zeolite catalyst.[7] The conclusion that no organic radicals are present in Y–R is also strongly supported by the observation that the EPR signal remains after calcination of the Y–R sample at an elevated temperature (as discussed later). Therefore, there are only two possibilities for the appearance of the singlet EPR signal in our samples: One is the formation of coke deposits within the zeolite pores or on the external surface of the zeolite;[8] the other possibility is the generation of paramagnetic centers in the framework of the zeolite. To further elucidate the origin of the EPR signal, we conducted a series of experiments.

First, we recorded infrared spectra of the Y–R sample and of the same sample after exposure to moisture. Neither of the coke absorption bands at around 1600 and 1540 cm^{-1} were detected,[9] whereas three typical CH deformation bands ($\delta_{as}(CH_2)=1453$ cm^{-1}; $\delta_s(CH_3)=1389$ cm^{-1}; and $\delta_s(CH_2)=1364$ cm^{-1}) were observed in the IR spectrum of the Y–R material (see Figure S8 in the Supporting Information). These IR bands vanished when the zeolite was exposed to moisture. The IR spectra indicate that no coke species are formed, but organic groups do exist in the Y–R material. The -CH_3 and -CH_2 absorption bands may be due to ethyl groups attached to the zeolite walls [Eq. (1), in which Zeo-O-H stands for HY][10]

$$\text{Zeo-O-H} + C_2H_5Br \rightarrow \text{Zeo-O-}C_2H_5 + HBr \quad (1)$$

and a small quantity of adsorbed ethyl bromide in HY after the L–S reaction. These ethyl groups can be removed by moisture through the formation of ethanol [Eq. (2)].[11]

$$\text{Zeo-O-}C_2H_5 + H_2O \rightarrow C_2H_5OH + \text{Zeo-O-H} \quad (2)$$

Second, we found that the pink-colored zeolite sample turned white again as soon as the material was exposed to the vapor of pure water (the dissolved oxygen in water was removed by a freeze–pump–thaw procedure). This process was accompanied by the disappearance of the singlet EPR signal. More importantly, the distinct EPR signal reappeared when the moisture-exposed Y–R sample was evacuated again to remove the adsorbed water molecules, whereas the Y–R material remained white after this treatment. This observation indicates that the color of the sample does not correlate with the EPR signal of the zeolite material. We monitored the color change of the zeolite sample during the L–S reaction by UV/Vis diffuse reflectance spectroscopy (see Figure S9 in the Supporting Information), which revealed that the color originates from the interaction between the zeolite-attached alkyl groups and the alkyl halide molecules: the heavier the halogen element involved, the deeper the color of the sample (see Figure S10 in the Supporting Information).

Additionally, we calcined the Y–R sample in air at 550 °C for 5 h, followed by evacuation at 200 °C for another 5 h. After this treatment, the alkyl groups had been completely decomposed, but the framework of zeolite Y remained intact, as confirmed by powder X-ray diffraction (Figure 2a). The intensity of the (111) diffraction peak is distinctly lower for the Y–R sample than for pristine HY and the calcined material (Y-calcined) owing the presence of the alkyl groups

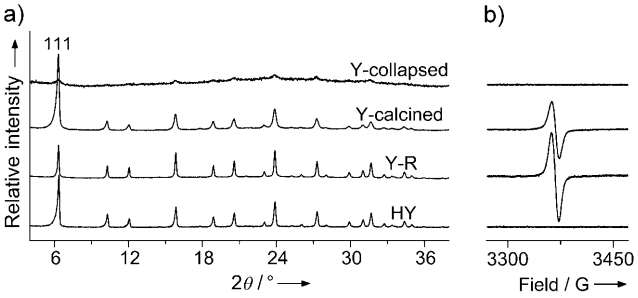

Figure 2. a) Powder X-ray diffraction patterns of zeolite HY, zeolite Y–R, and the Y–R sample after calcination; b) corresponding EPR spectra.

formed in the zeolite pores during the L–S reaction. Although thermal treatment removes the alkyl groups in the zeolite material, it has little influence on the singlet EPR signal if the HY sample remains crystalline (Figure 2b). However, the EPR signal disappears if the crystalline structure of the HY collapses (Y-collapsed) when the sample is heated rapidly to 550 °C. These observations indicate that the presence of the alkyl groups in the HY does not give rise to the singlet EPR signal, and that the paramagnetic centers must be in the framework of the zeolite after the L–S reaction.

The framework of a typical zeolite HY has an empirical composition $[Si_{1-x}Al_xO_2]^{x-}$, the negative charges of which are compensated by protons. The silicon and aluminum centers in the zeolite framework are already in their respective highest oxidation states, and the protons can not be further oxidized either. However, the oxidation state of the lattice oxygen atoms is −2, and in principle it is possible to oxidize the lattice oxygen atoms to higher-oxidation-state species (−1 or 0).

Therefore, the paramagnetic centers in the framework of the zeolite may be associated with the framework oxygen atoms, from which electrons are transferred to the reactant molecules during the L–S reaction.

To pinpoint the process that accounts for the formation of the paramagnetic centers, we split the L–S reaction process into two steps. The zeolite HY was first exposed to ethyl bromide vapor at 50 °C for 24 h (see Figure S11 in the Supporting Information). We refer to this process as the "gas–solid" (G–S) reaction. After the G–S reaction, the color of the zeolite was again light pink. Also, the IR and the UV/Vis spectra of the HY sample after the G–S reaction (see Figures S8 and S9 in the Supporting Information) were identical to those of the sample after the L–S reaction, which suggests that the O-bonded alkyl groups formed during these two reactions are the same. However, the EPR spectrum of the HY material after the G–S reaction was completely silent, and only ethene and hydrogen bromide were detected in the gas phase of the reaction product (see Figure S12 in the Supporting Information). Thus, it is believed that the G–S reaction leads to the formation of O-bonded ethyl groups by the reaction pathway in Equation (1). Some of the O-bonded ethyl groups undergo dissociation to form ethene, and the bridging O atoms are protonated again [Eq. (3)].

$$\text{Zeo-O-C}_2\text{H}_5 \rightarrow \text{Zeo-O-H} + \text{C}_2\text{H}_4 \qquad (3)$$

After this step, no electron transfer from the framework O atoms to the organic molecules occurs, and hence no paramagnetic centers can be detected. Nevertheless, after the second step, when the HY after the G–S reaction is stirred with liquid ethyl bromide for several hours at 50 °C, both the singlet EPR signal for the zeolite and ethane appear. This observation indicates that the generation of paramagnetic centers is closely related to the formation of ethane in the reaction system. Evidently, the ethyl bromide liquid plays the role of a "carrier" during the generation of paramagnetic centers. That is, the ethyl bromide molecules in the liquid phase carry the ethyl radicals ($C_2H_5^{\bullet}$) away from the O-bonded sites to leave electron-deficient O atoms in the zeolite framework. To confirm this speculation, we submerged the HY zeolite after the G–S reaction into various liquid alkyl halides instead of ethyl bromide. We found that all the solvents tested help the zeolite to produce paramagnetic centers and ethane. Thus, the formation of paramagnetic centers does not depend on the chemical composition of the carrier, as long as it can bring the ethyl radicals away from the zeolite walls.

The formation of ethane from ethyl radicals may follow three pathways. In the first, the ethyl radical abstracts a hydrogen atom from the Brønsted acid site to form ethane, with the generation of a paramagnetic center at a framework O atom that bridges an Si and an Al atom. In a second pathway, the ethyl radical abstracts another ethyl radical bonded to an O atom that bridges an Si and an Al atom, with the formation of ethene and ethane through a disproportionation reaction. This pathway also results in the formation of a paramagnetic center at an Si,Al-bridging O atom. The third pathway is a process involving electron transfer from a framework oxygen atom that bridges two Si atoms.

To identify the correct pathway, we used the zeolites HX (protonated zeolite X; see Figure S13 in the Supporting Information) with a framework Si/Al ratio of 1.20 and H-SAPO-44 (protonated zeolite SAPO-44 with a chabazite structure; see Figure S14 in the Supporting Information) in place of HY and examined the resulting EPR signals. A singlet EPR signal, the position of which was identical to that for HY, was observed for HX after a similar L–S reaction, which indicates that the same mechanism for the formation of paramagnetic centers was effective in these two zeolite materials (see Figure S15 in the Supporting Information). Zeolite X has the same crystal structure as Y, but the Si/Al ratio of X is distinctly smaller than that of Y. In HX, most of the framework oxygen atoms are linked to an Al center, whereas those bridging two Si atoms are rare. After protonation, the concentration of Brønsted acid sites in HX is higher than in HY. If electron abstraction occurs from O atoms bridging an Si and an Al atom, the EPR signal for the HX sample should be stronger than that for the HY material after the L–S process. However, the EPR signal intensity of HX is much weaker than that of HY after the L–S reaction (see Figure S16 in the Supporting Information). SAPO-44 is a microporous silicoaluminophosphate in which almost all framework Si atoms are linked to four Al atoms through an oxygen atom, because the Si centers and P atoms are in equivalent positions. In other words, the amount of oxygen atoms bridging two framework Si atoms is negligible in this material. No EPR signal and no ethane were detected for H-SAPO-44 after the L–S reaction. These observations are in agreement with the mechanism in which electron abstraction after the L–S reaction is from oxygen atoms between two Si atoms, rather than from those bridging an Si and an Al atom in the zeolite framework.

Quantum-chemical calculations gave the optimized structure of the initially formed O-bonded ethyl groups linked to ethyl bromide in the pores of zeolite Y (Figure 3).[12] According to the calculation results (see Table S1 in the Supporting Information), the ethyl bromide molecule is strongly attracted to both the ethyl group and a nearby lattice O atom bridging two Si atoms; thus, a ring structure is formed. This ring structure exists after both the G–S and the L–S reactions. In the presence of an organic liquid as a carrier, the ring can be broken, and the ethyl bromide molecule leaves the zeolite wall with an electron abstracted from the oxygen atom that bridges two Si atoms. At the same time, the ethyl group draws the bromine atom from the leaving ethyl bromide molecule to form a new ethyl bromide molecule and a new ethyl radical. The ethyl radical can then interact with another radical in a liquid medium to produce ethene and ethane.

Halogen-switch reactions over zeolites, that is, the transfer of a halogen atom from one molecule to another under the assistance of a zeolite material, have been reported recently.[13] Similarly, in our system, it is possible for the bromine atom to shift from the ethyl bromide molecule to the adjacent O-bonded ethyl group. To confirm this reactivity, we treated the dehydrated HY with 2-chloropropane vapor in the

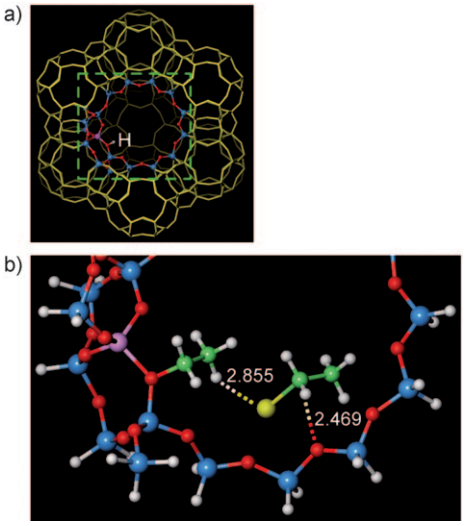

Figure 3. a) Structure of zeolite Y with the cluster model used in this study. b) B3P86/6-31g*-optimized geometry of the O-bonded ethyl group linked to an ethyl bromide molecule through an electrostatic effect (distances: 2.855 and 2.469 Å; red O, blue Si, purple Al, green C, yellow Br, white H.)

G–S reaction, and then stirred the HY material in liquid ethyl bromide for several hours at 50 °C. After this reaction, 2-bromopropane was detected: the product of bromine transfer from ethyl bromide to the isopropyl group attached to the zeolite wall [Eq. (4)]. This observation clearly demonstrates

$$\text{Zeo-O-}i\text{-}C_3H_7 + C_2H_5Br \rightarrow \text{Zeo-O-}C_2H_5 + i\text{-}C_3H_7Br \quad (4)$$

that the bromine atom can be transferred from an alkyl bromide molecule to an O-bonded alkyl group in a zeolite. This bromine shift renders it possible for the framework electron to be lost from an O atom bridging two Si atoms, rather than from an O atom bridging an Si and an Al atom.

The density of paramagnetic sites for different zeolite samples after the L–S reaction varies to a considerable extent (see Table S2 in the Supporting Information). The HY sample shows the highest paramagnetic site density among all the zeolite materials. As NaX has no Brønsted acid sites, this material is not able to react with ethyl bromide, and therefore no paramagnetic sites can be generated in NaX. In H-SAPO-44 or HX, the amount of Si,Si-bridging oxygen atoms is negligible or very small, and therefore the paramagnetic signal in these two materials is either unobservable or relatively weaker, as pointed out earlier. Although H-mordenite and Hβ both contain sufficient Si,Si-bridging oxygen atoms, the concentration of Brønsted acid sites in these zeolites is much lower than in HY because of their high Si/Al ratio. Therefore, the density of paramagnetic centers generated in these materials according to the mechanism described above is also lower than in HY.

The paramagnetic centers on the framework of zeolites are chemically accessible. When the HY material was exposed to NO after the L–S reaction, the IR bands of NO^+ (2210 and 2142 cm^{-1}) were identified,[14] and the intensity of the EPR signal decreased (Figure 4; see also Figure S17 in the Supporting Information). This observation indicates that the hole on the framework oxygen atom can readily capture the unpaired electron of NO. The evacuation of NO from the

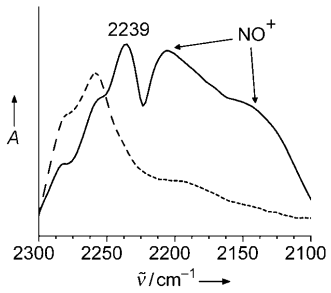

Figure 4. FTIR spectra of the HY sample after the L–S reaction (dotted line) and upon exposure to gaseous NO at room temperature (solid line). The appearance of the band at 2239 cm^{-1} after the adsorption of NO is due to the presence of a minor amount of N_2O, which does not interact with the paramagnetic centers, as an impurity.

system resulted in the recovery of the paramagnetic centers and the disappearance of the IR bands of the NO^+ species. This result suggests that the interaction between the NO molecule and the hole on the framework O atom is reversible. Methanol, which is a good electron donor, also interacted with the paramagnetic centers: The treatment of the Y–R system with methanol led to the appearance of an EPR signal due to the methyleneoxonium radical ($CH_2OH_2^{+\bullet}$),[15] with five hyperfine lines (see Figure S18 in the Supporting Information). On the other hand, O_2, N_2O, and CCl_3F, which are typical electron acceptors, did not interact with the paramagnetic centers in the zeolite sample. These results clearly indicate that the paramagnetic centers of the Y–R zeolite sample are holes rather than unpaired electrons.

In summary, a process of electron transfer from a zeolite framework to organic molecules has been established experimentally. A distinct singlet EPR signal was detected for the resulting zeolite for the first time, and the reduction of an alkyl bromide to its corresponding alkane was observed. Our finding shows that zeolites in a protonated form function not only as acid catalysts but also as electron donors upon interaction with alkyl halide molecules.

Experimental Section

The L–S and G–S reactions are described in the Supporting Information.

Control experiments: The zeolites NaX, HX, Hβ, H-mordenite, and H-SAPO-44 were also used as catalysts in the L–S and G–S reactions with ethyl bromide. Detailed procedures for the preparation and characterization of these zeolites are provided in the Supporting Information.

Characterization**:** The powder X-ray diffraction (XRD) patterns were recorded on a Rigaku D/Max 2550 X-ray diffractometer with $Cu_{K\alpha}$ radiation ($\lambda = 1.5418$ Å). The EPR spectra were obtained on a JES-FA 200 EPR spectrometer. The instrumental parameters were as follows: scanning frequency, 9.45 GHz; central field, 3371.44 G; scanning width, 8000 G; scanning power, 0.998 mW; scanning temperature, 25 °C. 2,2-Diphenyl-1-picrylhydrazyl (DPPH) was used as a

reference for the calculation of spin concentration. For in situ infrared measurements, a thin self-supporting wafer (10–15 mg cm^{-2}) of the sample was evacuated in the preheating zone of a home-made IR cell by heating the sample to 250 °C for 2 h. When the sample had cooled to room temperature, it was lowered from the preheating zone into the sample compartment for IR measurement. The sample in the IR cell was then exposed to NO, and the IR spectrum was recorded again for comparison. For investigations into the effect of water on the zeolite material after the L–S and G–S reactions, a thin layer of the powder sample was sandwiched evenly between two CaF_2 plates in a glove box, and the plates were then sealed with Parafilm to avoid moisture in the air. Subsequently, the sample between the sealed plates was taken out of the glove box and mounted on the FTIR spectrometer for measurements. Finally, the Parafilm was removed from the CaF_2 plates to expose the sample to moist air, and the IR spectrum of the sample was recorded again. All FTIR spectra were recorded on a Bruker IFS 66v/S FTIR spectrometer equipped with a deuterated triglycine sulfate (DTGS) detector. UV/Vis diffuse reflectance spectra were recorded on a Perkin–Elmer Lambda 20 UV/Vis spectrometer. Absorbance spectra were obtained from the reflectance spectra through Kubelka–Munk transformation. Temperature-dependent magnetic-susceptibility data were recorded on a Quantum Design MPMS-XL SQUID magnetometer. Magic-angle spinning (MAS) ^{29}Si NMR measurements were made with a Varian Infinity Plus 400 NMR spectrometer. A Perkin–Elmer Optima 3300DV ICP spectrometer was used for elemental analysis.

Received: April 24, 2009
Published online: August 7, 2009

Keywords: alkyl halides · electron transfer · EPR spectroscopy · redox sites · zeolites

[1] a) A. Corma, *Chem. Rev.* **1995**, *95*, 559 – 614; b) M. E. Davis, *Nature* **2002**, *417*, 813 – 821.
[2] G. Busca, *Chem. Rev.* **2007**, *107*, 5366 – 5410.
[3] M. J. Nash, A. M. Shough, D. W. Fickel, D. J. Doren, R. F. Lobo, *J. Am. Chem. Soc.* **2008**, *130*, 2460 – 2462.
[4] D. N. Stamires, J. Turkevich, *J. Am. Chem. Soc.* **1964**, *86*, 757 – 761.
[5] K. B. Yoon, *Chem. Rev.* **1993**, *93*, 321 – 339.
[6] a) H. G. D. Mcmanus, C. Finel, L. Kevan, *Radiat. Phys. Chem.* **1995**, *45*, 761 – 764; b) M. Alvaro, H. Garcia, S. Garcia, F. Marquez, J. C. Scaiano, *J. Phys. Chem. B* **1997**, *101*, 3043 – 3051; c) S. Hashimoto, *J. Chem. Soc. Faraday Trans.* **1997**, *93*, 4401 – 4408; d) Y. S. Park, S. Y. Um, K. B. Yoon, *J. Am. Chem. Soc.* **1999**, *121*, 3193 – 3200.
[7] H. Garcia, H. D. Roth, *Chem. Rev.* **2002**, *102*, 3947 – 4007.
[8] a) J.-P. Lange, A. Gutsze, H. G. Karge, *J. Catal.* **1988**, *114*, 136 – 143; b) H. G. Karge, J. P. Lange, A. Gutsze, M. Laniecki, *J. Catal.* **1988**, *114*, 144 – 152.
[9] F. Bauer, H. G. Karge in *Molecular Sieves—Science and Technology*, *Vol. 5* (Eds.: H. G. Karge, J. Weitkamp), Springer, Berlin, **2006**, chap. 5.
[10] a) M. T. Aronson, R. J. Gorte, W. E. Farneth, D. White, *J. Am. Chem. Soc.* **1989**, *111*, 840 – 846; b) M. Boronat, P. M. Viruela, A. Corma, *J. Am. Chem. Soc.* **2004**, *126*, 3300 – 3309.
[11] W. Wang, J. Jiao, Y. J. Jiang, S. S. Ray, M. Hunger, *ChemPhysChem* **2005**, *6*, 1467 – 1469.
[12] See the Supporting Information.
[13] a) Y. J. Jiang, M. Hunger, W. Wang, *J. Am. Chem. Soc.* **2006**, *128*, 11679 – 11692; b) M. Franco, N. Rosenbach, Jr., G. B. Ferreira, A. C. O. Guerra, W. B. Kover, C. C. Turci, C. J. A. Mota, *J. Am. Chem. Soc.* **2008**, *130*, 1592 – 1600.
[14] C. Henriques, O. Marie, F. Thibault-Starzyk, J. C. Lavalley, *Microporous Mesoporous Mater.* **2001**, *50*, 167 – 171.
[15] a) J. F. Gibson, M. C. R. Symons, M. G. Townsend, *J. Chem. Soc.* **1959**, 269 – 276; b) D. R. G. Brimage, J. D. P. Cassell, J. H. Sharp, M. C. R. Symons, *J. Chem. Soc. A* **1969**, 2619 – 2621.

